applied sciences

MDPI

Article

Numerical Analysis of Human Cancer Therapy Using Microwave Ablation

Marwa Selmi [1,2,*], Abdul Aziz Bin Dukhyil [3] and Hafedh Belmabrouk [2,4]

1 Department of Radiological Sciences and Medical Imaging, College of Applied Medical Sciences, Majmaah University, Al Majmaah 11952, Saudi Arabia
2 Laboratory of Electronics and Microelectronics, Faculty of Science of Monastir, University of Monastir, Environment Boulevard, Monastir 5019, Tunisia; ha.belmabrouk@mu.edu.sa
3 Department of Medical Laboratory Sciences, College of Applied Medical Sciences, Majmaah University, Al Majmaah 11952, Saudi Arabia; a.dukhyil@mu.edu.sa
4 Department of Physics, College of Science, Majmaah University, Zulfi 11932, Saudi Arabia
* Correspondence: m.selmi@mu.edu.sa; Tel.: +966-563447961

Received: 26 November 2019; Accepted: 24 December 2019; Published: 26 December 2019

Featured Application: This study developed a computer simulation based on the finite element method to investigate microwave ablation performance, antenna design, electromagnetic and thermal effects, specific absorption rate (SAR), and fraction of necrotic tissue within cancer treatment. The numerical results show that SAR and temperature distribution are strongly affected by input microwave power. High microwave power causes a high SAR value and raises the temperature above 50 °C, which may destroy healthy cells.

Abstract: Microwave ablation is one type of hyperthermia treatment of cancer that involves heating tumor cells. This technique uses electromagnetic wave effects to kill cancer cells. A micro-coaxial antenna is introduced into the biological tissue. The radiation emitted by the antenna is absorbed by the tissue and leads to the heating of cancer cells. The diffuse increase in temperature should reach a certain value to achieve the treatment of cancer cells but it should be less than a certain other value to avoid damaging normal cells. This is why hyperthermia treatment should be carefully monitored. A numerical simulation is useful and may provide valuable information. The bio-heat equation and Maxwell's equations are solved using the finite element method. Electro-thermal effects, temperature distribution profile, specific absorption rate (SAR), and fraction of necrotic tissue within cancer cells are analyzed. The results show that SAR and temperature distribution are strongly affected by input microwave power. High microwave power causes a high SAR value and raises the temperature above 50 °C, which may destroy healthy cells. It is revealed that with a power of 10 W, the tumor cells will be killed without damaging the surrounding tissue.

Keywords: heat transfer; hyperthermia treatment; micro-coaxial antenna; tumor cancer

1. Introduction

Cancer tumors in the liver, breast, kidney, bone, lung, and other organs are the largest causes of death in the world. Furthermore, thinking about cancer remains scary. Annually, over 411,000 deaths result from breast cancer [1]. Lung cancer is one of the leading causes of death in the United States, accounting for more than 160,000 deaths per year [2]. In addition, liver cancer is one of the most significant health issues leading to death worldwide [3]. Each year, more than a million deaths of people result from this disease. Skin cancer is one of the most common cancer types in Saudi Arabia. It accounted for 3.2% of all treated cancer cases in 2010 [4]. Techniques of cancer treatment are

undergoing continuous development and are still a current research topic for scientific researchers as well as for doctors working on the clinical detection and treatment of diseases. In recent years, there has been a great amount of attention paid to the development of cancer treatment methods. Furthermore, many techniques are widely used for saving patients. However, new techniques are also welcomed, since they may bring particular contributions and added value to available techniques.

Hyperthermia is a cancer treatment that takes advantage of the heating of tumor cells in the body at a definite level. Indeed, raising the temperature of tumor cells causes lesions of the cell membrane which leads to destruction of the cancer cells [5,6]. Research on hyperthermia as an anti-cancer treatment has been in place for many years. Nowadays, hyperthermia is utilized as a complement to radiotherapy and chemotherapy. Cancer treatment using hyperthermia necessitates the generation of an adequately controlled amount of heat inside the cancerous tumor. If it is exposed to a temperature of approximately 52 °C for one hour, the cancer tissue can be damaged [7–11]. The amount of dissipated heat should be used prudently. However, if a large amount of heat is administrated, the skin or other healthy tissue could be destroyed. A versatile clinical hyperthermia system is adapted to microwaves for cancer treatment inside the body. The energy radiated by a microwave is an effective way to heat the tumor. Indeed, since the tissue is an electrically conductive material, a part of this radiated energy is dissipated inside the tissue and leads to the increase of its temperature. In addition, microwaves can be provided to the tissue by specific antennas situated close to or inserted into the tissue to be treated. According to the size of the tumor and the location in the body, one or more microwave antennas can be used to treat the tumor. When a microwave antenna is activated, the tissues which have water content and which are exposed to large amounts of microwave energy heat up. An adequate calibration of the microwave energy can heat the tumor and protect healthy tissues.

Cancer treatment techniques have been extended during the past several years because the killing of cancer tumors is difficult to achieve with surgery. The ablative treatment family includes microwave ablation (MWA), radiofrequency ablation (RFA), ethanol ablation, laser ablation, and cryoablation [12–17]. Recently, a wide number of experimental and theoretical works have been focused on improving MWA [18–27].

Yingxu et al. (2017) have studied, in their numerical and experimental research, the performance of a tri-slot antenna, and have compared it with a single slot antenna with an operating frequency of 433 MHz [22]. They demonstrated that the tri-slot antenna which had a frequency of 433 MHz created a gourd-shaped MWA area with a longer length. Curto et al. (2015) have presented a comparative study between the differences in microwave ablation at 915 MHz and 2.45 GHz, with a power of 30 W used at the antenna input [21]. Their results indicated that a greater ablation zone is created when using a coaxial antenna with a single slot at 2.45 GHz. However, the models used by Curto et al. and Yingxu et al. did not take into account any change in tissue properties such as tissue water vaporization, vapor condensation, and tissue shrinkage [21,22].

Tao et al. (2015) have presented a numerical evaluation of the heat transfer process in liver tumors according to temperature-dependent properties using a coaxial antenna with ten slots [25]. Their simulations showed that using a coaxial multi-slot antenna reduces over-treatment compared with a conventional coaxial antenna. In addition, they revealed that a coaxial antenna with multi-slots generates the smallest over-treatment region for spherical tumors. Rubio et al. (2015) performed a computer simulation in order to compare heating differences between cancer and normal breast tissue [26]. They demonstrated that the dielectric and thermal parameters relative to cancer and normal breast tissue are able to create special heating of tumors during microwave ablation. Although the available computational models provide a strategy for cancer treatment, they require further development.

Numerical modeling remains primordial when it comes to carrying out a parametric study, evaluating the importance of the inherent phenomena, and leading to better optimization of the design of new devices. For example, clinical treatment with MWA requires the control of elevation of temperature in order to ensure the destruction of cancer cells without damaging healthy tissue. Hence,

numerical simulation has been widely used in the investigation of MWA as an instructive tool guiding practical treatment.

In the present work we have investigated the interaction between electromagnetic waves with tissue in order to treat liver cancer. A two-dimensional numerical simulation is performed using the finite element method. Maxwell's equations and the bio-heat equation are used to estimate the electric field and the heat distribution in the liver tissue. Heat generation by the antenna is used to destroy cancer cells but high temperature can damage healthy surrounding tissue. In addition, the influence of input microwave power, specific absorption rate (SAR), and temperature distribution on the liver tissue, and the fraction of necrotic tissue during the ablation thermal, are investigated.

2. Description and Formulation of the Problem

2.1. Thermal Problem

The biological tissue investigated is the liver. A micro-coaxial antenna is used to generate an electric field. The heat transfer problem in the biological medium is described by the bio-heat equation [28]

$$\rho C_p \frac{\partial T}{\partial t} = \nabla(k\nabla T) + \rho_b C_b \omega_b (T_b - T) + Q_{ext} + Q_{meta} \tag{1}$$

where T is the tissue's temperature, ρ is its density, C_p is its specific heat capacity, k is its thermal conductivity, $\rho_b = 1060$ kg·m^{-3} is the blood density, $C_b = 3600$ Jkg^{-1} denotes the specific heat capacity of the blood, ω_b represents the blood perfusion rate, and T_b is the blood temperature. In this study, we assume $T_b = 37$ °C.

The first term in Equation (1) represents the transient term whereas the second term denotes the heat conduction. The third term represents the heat dissipation by the blood flow. Q_{ext} denotes the external heat source and Q_{meta} is the heat source from the metabolism. The value of Q_{meta} is usually neglected compared to the other heat terms.

The external source term Q_{ext} results from the heat generated by the electromagnetic field, i.e.,

$$Q_{ext} = \frac{\sigma}{2}\|E_0\|^2 \tag{2}$$

where σ denotes the electric conductivity of the biological tissue (S/m) and E_0 is the amplitude of the electric field generated by the micro-coaxial antenna.

The thermal conductivity, density, and specific heat of the liver are dependent on temperature. Their expressions can be extracted from the literature [29]. For the normal tissue, we have

$$k_{liver}(T) = 4190[0.133 + 1.36W_a(T)] \tag{3}$$

$$\rho_{liver}(T) = 1300 - 300W_a(T) \tag{4}$$

$$C_{p,liver}(T) = 0.419[0.37 + 0.63W_a(T)] \tag{5}$$

In the above equations, the temperature is expressed in degrees Celsius. The parameter $W_a(T)$ is the measured remaining tissue water content versus temperature of the liver tissue [30]. It is given by

$$W_a(T) = \begin{cases} 0.778 - 0.779 \times \exp\left(\frac{T-106}{3.42}\right) & T \leq 103\ ^\circ\text{C} \\ -0.03924(T-103) + 0.454392 & 103\ ^\circ\text{C} < T \leq 104^\circ\text{C} \\ 0.778 \times \exp\left(-\frac{T-80}{34.37}\right) & T > 104\ ^\circ\text{C} \end{cases} \tag{6}$$

Figure 1 depicts the evolution of the quantities $W_a(T)$, $k_{liver}(T)$, $\rho_{liver}(T)$, and $C_{p,liver}(T)$ versus the temperature T. It is clear that these quantities remain almost constant when the temperature T is smaller than 80 °C. For this reason we assume henceforth that the quantities k_{liver}, ρ_{liver}, and $C_{p,liver}$ are constant and do not vary with temperature. The condition $T < 80$ °C will be ensured.

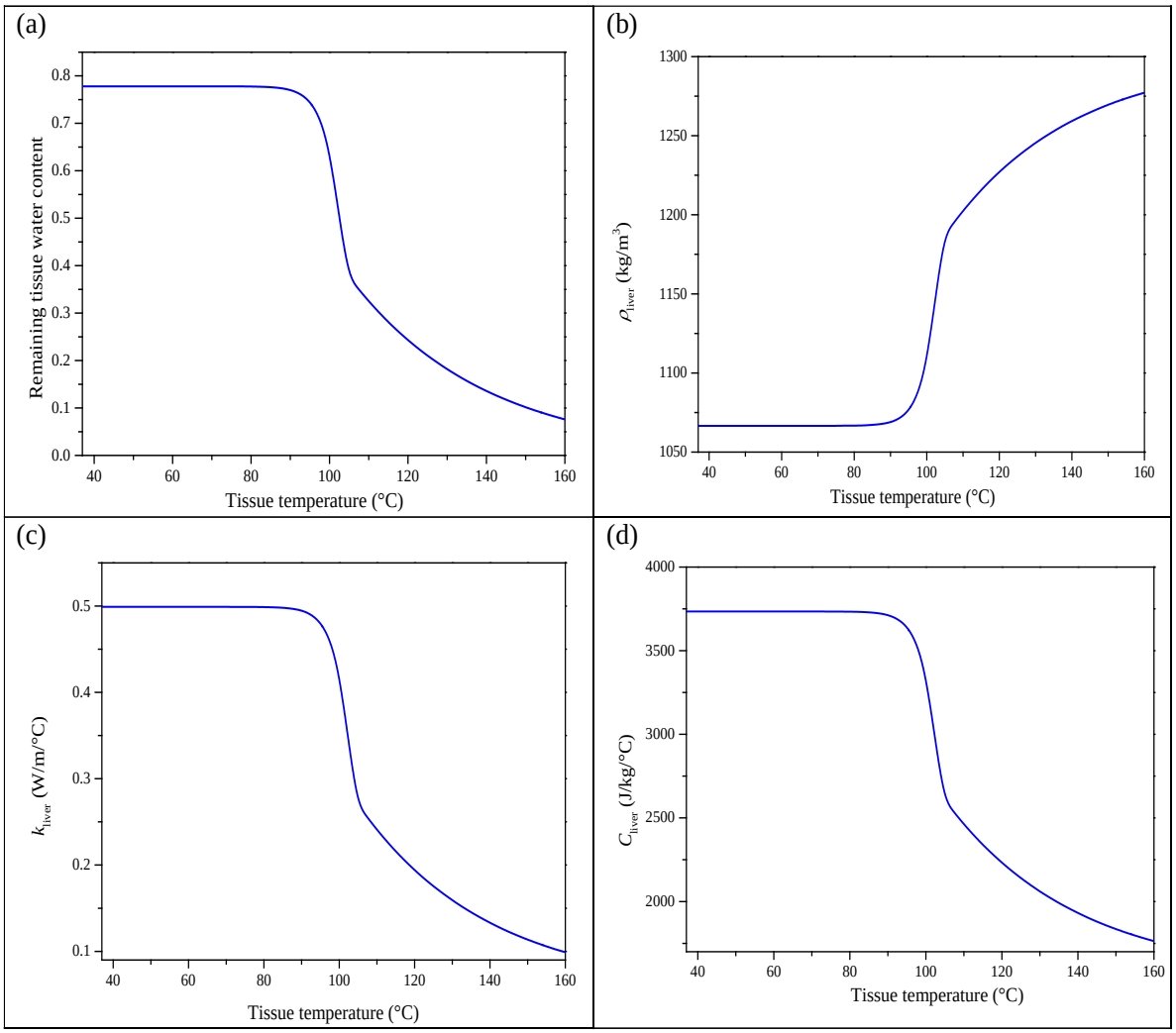

Figure 1. Evolution of thermal properties versus the temperature. (**a**) Remaining mass of tissue water $W_a(T)$, (**b**) density of the liver tissue $\rho_{liver}(T)$, (**c**) thermal conductivity of the liver tissue $k_{liver}(T)$, and (**d**) specific heat of the liver tissue $C_{p,liver}(T)$.

Regarding the properties of the tumor, we used the following values: $k_{tumor} = 0.57\,\mathrm{W/m\,°C}$, $\rho_{tumor} = 1040\ \mathrm{kg\,m^{-3}}$, and $C_{p,tumor} = 3960\,\mathrm{J\,kg^{-1}\,K^{-1}}$. These values are independent of the temperature [7].

The blood flow induces a convective heat flux between the blood flow and the tissue. This heat flux depends on the temperature difference $(T_b - T)$ and the blood flow rate. Hence, it is influenced by blood perfusion [31]. It is represented by the term $\rho_b C_b \omega_b (T_b - T)$. The rate of blood perfusion versus temperature is given by

$$\omega_b(T) = \omega_0 + a\,T \tag{7}$$

In the above equation, T is also expressed in degrees Celsius, whereas the unit of the rate ω_b is $\mathrm{s^{-1}}$. The constants involved in Equation (7) are given by $\omega_0 = 6.08 \times 10^{-3}\ \mathrm{s^{-1}}$ and $a = 2.1 \times 10^{-5}\ \mathrm{s^{-1}\,°C^{-1}}$.

The source term in Equation (1) depends on the electric field amplitude. The next paragraph will explain how this quantity is computed.

2.2. Electromagnetic Problem

In order to heat the tumor and provoke its ablation, a micro-coaxial antenna is inserted into the tissue. This antenna radiates an electromagnetic wave. This wave is assumed to be axisymmetric (i.e., the components of the electric and magnetic fields do not depend on the azimuthal angle φ) and

transverse magnetic. The magnetic field of this wave has only the azimuthal component, $H = H_\varphi \boldsymbol{e}_\varphi$, where $\boldsymbol{e}_\varphi$ is the azimuthal unit vector. The azimuthal component is expressed by $H_\varphi = H_0(r,z)e^{j(\omega t - kz)}$, where r, φ, and z are the cylindrical coordinates, ω denotes the angular frequency of the wave, and k is the wave number.

The liver and the tumor are assumed to be non-ideal dielectrics characterized by their relative permittivity ε_r, electric conductivity σ, and relative permeability μ_r. In the range of temperature 37 °C ≤ T ≤ 100 °C, these quantities are given by [3,32,33]

$$\varepsilon_{r,\,liver}(T) = 47.043 - 0.042\,T \tag{8}$$

$$\sigma_{liver}(T) = 1.7381 - 0.0004\,T \tag{9}$$

$$\varepsilon_{r,\,tumor}(T) = 48.16 \tag{10}$$

$$\sigma_{tumor}(T) = 2.09 \tag{11}$$

$$\mu_{r,liver} = \mu_{r,tumor} = 1 \tag{12}$$

Since the temperature depends on the position, it appears that the electric properties also depend on the position. In other words, when writing Maxwell's equations, some care should be taken. It is straightforward to show that the magnetic field of the wave is governed by the following expression

$$\nabla \times \left(\left(\varepsilon_r - \frac{j\sigma}{\omega \varepsilon_0} \right)^{-1} \nabla \times \vec{H}_\varphi \right) - \mu_r \frac{\omega^2}{c^2} \vec{H}_\varphi = 0 \tag{13}$$

where $\varepsilon_0 = 8.8542 \times 10^{-12}$ F/m and c is the speed of light in a vacuum.

The components of the electric field are obtained by

$$\begin{cases} E_r = -\frac{1}{\sigma + j\omega\varepsilon_0\varepsilon_r} \frac{\partial H_\varphi}{\partial z} \\ E_\varphi = 0 \\ E_z = \frac{1}{\sigma + j\omega\varepsilon_0\varepsilon_r} \frac{1}{r} \frac{\partial (rH_\varphi)}{\partial r} \end{cases} \tag{14}$$

2.3. Geometry of the Liver and the Inserted Antenna

The thermal microwave ablation treatment consists of using heat to kill tumor cells in a tumor. It involves the use of a microwave coaxial antenna (MCA) immersed in biological tissue (see Figure 2). This antenna radiates energy throughout the biological tissue. This energy is converted into heat, which invades the tissues. The MCAs are largely used for their advantages, namely, low manufacturing cost, reduced dimensions, simple design, and utility for treatment [34]. The antenna is formed by an inner conductor (diameter 0.135 mm), a dielectric (diameter 0.335 mm), and an outer conductor (diameter 0.460 mm) containing a ring-shaped slot with a height of 1 mm. A plastic catheter (diameter 0.895 mm) surrounds the antenna. The antenna operates with a frequency of 2.45 GHz. The dimensions of the antenna are given in Figure 3. The relative permittivity values of the dielectric and catheter are 2.03 and 2.1, respectively. The tumor is considered to be a sphere with a 10 mm radius.

The simulation domain used is shown in Figure 3. It contains two areas, namely, the normal tissue and the tumor. The normal tissue is the liver and it is assumed to have a cylindrical geometry, having a radius of 30 mm and a height of 80 mm. The antenna is implanted into the liver tissue. The depth of the insertion is 70.5 mm.

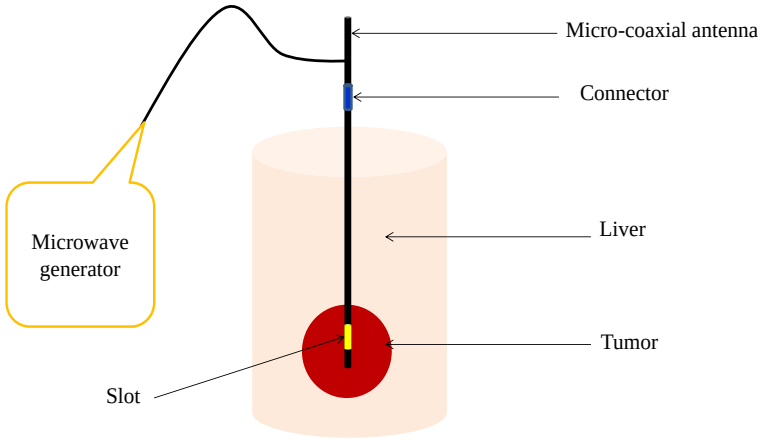

Figure 2. Schema of the antenna inserted into biological tissue.

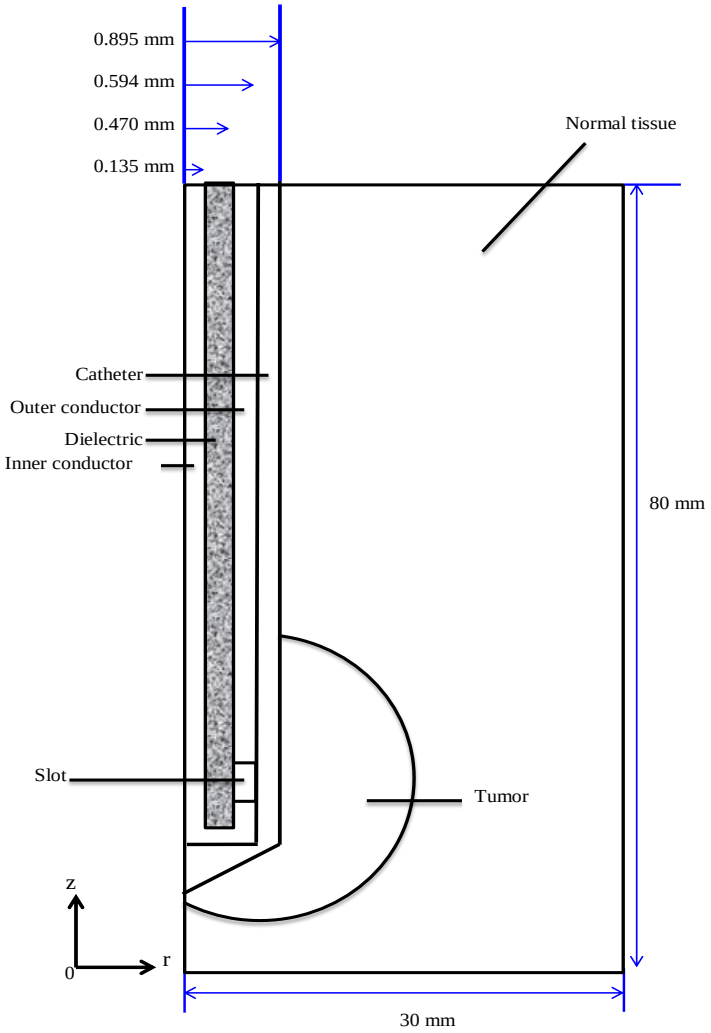

Figure 3. Axial schema of the micro-coaxial antenna inserted in biological tissue.

2.4. Boundary Conditions

i. The axis z is a symmetry axis.

ii. The insulation condition is applied to the surroundings of the liver. In other words, the heat flux through the surrounding walls is equal to zero. The mathematical equation expressing this condition may be written in a synthetic form, $\boldsymbol{n}.(k\nabla T) = 0$, where n is the unit vector normal to

the boundary ($z = 0$ or $z = 80$ mm or $r = 30$ mm). This condition can be further specified for each boundary, i.e.,

$$k\frac{\partial T}{\partial z}\Big|_{z=0\text{mm}} = 0;\ k\frac{\partial T}{\partial z}\Big|_{z=80} = 0;\ k\frac{\partial T}{\partial r}\Big|_{r=30\text{mm}} = 0$$

Indeed, the unit normal vector is equal, respectively, to the axial vector $\boldsymbol{e}_z$ and the radial vector $\boldsymbol{e}_r$.

iii. The heat flux is continuous through the interface between the tissue and the tumor, i.e., $k_{liver}\nabla T_{liver} = k_{tumor}\nabla T_{tumor}$.

The boundary conditions used for the numerical simulation are presented in Figure 4. These boundary conditions concern the heat transfer equation and the electromagnetic field. With regard to the heat transfer equation, the following boundary conditions are used.

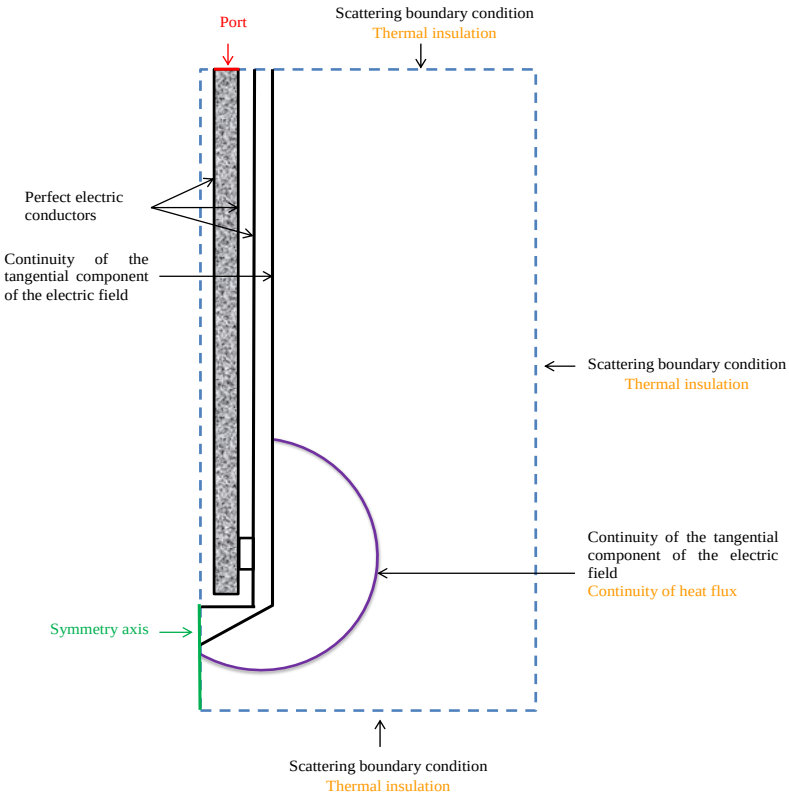

Figure 4. Boundary conditions used for the simulation.

Equation (1) also requires an initial condition. The initial temperature is assumed to be constant, i.e., $T(t = 0, r, z) = 37\ ^\circ\text{C}$.

The boundary conditions for the electromagnetic field are:

i. To the inlet of the antenna, an input microwave power is assigned.

ii. The z axis is a symmetry axis: $E_r(t, r = 0, z)$ and $\frac{\partial E_z}{\partial r}(t, r = 0, z)$.

iii. The scattering boundary condition is used at the surrounding of the liver: ($z = 0$ or $z = 80$ mm or $r = 30$ m).

iv. The walls of the antenna $r = 0.135$ mm or $r = 0.47$ mm or $r = 0.594$ mm are considered to be perfect electric conductors $\boldsymbol{n}.\boldsymbol{E} = 0$.

v. There is continuity of the tangential component of the electric field at the interface between the tissue and the tumor: $\boldsymbol{n} \wedge (\boldsymbol{E}_2 - \boldsymbol{E}_1) = 0$.

2.5. Numerical Method and Model Validation

The set of equations describing the electromagnetic wave propagation and the heat transfer can be solved by the finite element method (FEM) with the Galerkin approach [35]. To find the numerical solution of these coupled equations, a computer code was developed. The physical domain was composed of three subdomains, namely, the liver, the tumor, and the antenna. The axial symmetry 2D global domain was divided into triangular elements using Lagrange quadratic shape functions. The sensitive domain was refined with a better mesh quality.

Figure 5 displays a flow chart describing the simulation scheme. The coupling of the equations lies from the fact that the volumetric source term in the heat equation depends on the amplitude of the electric field, and, inversely, the relative permittivity and the electrical conductivity of the medium depend on the temperature. This is a two-way coupling.

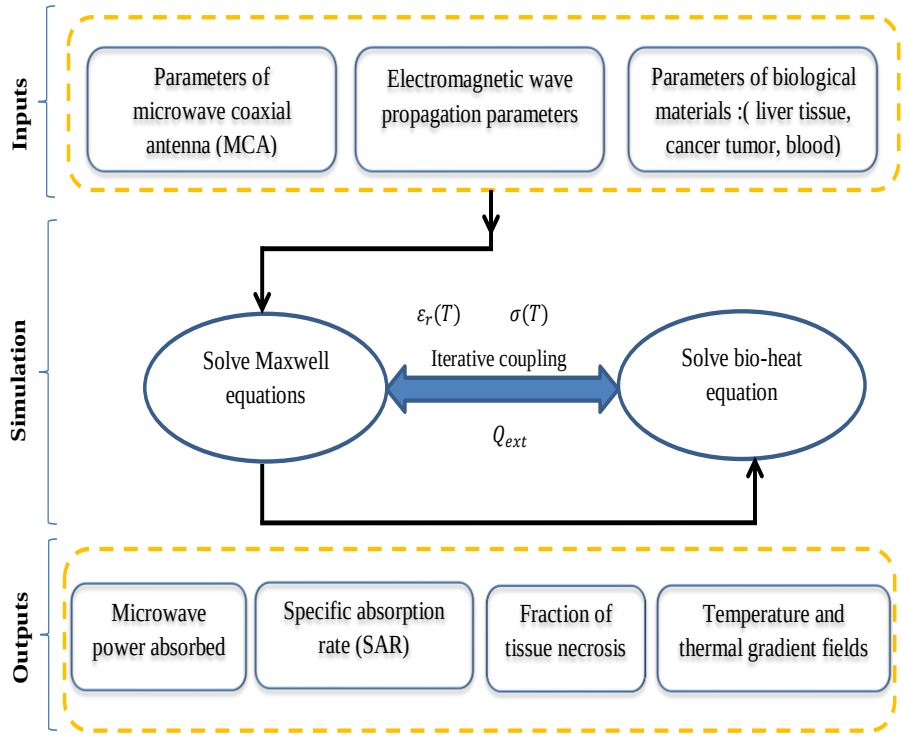

Figure 5. Flow chart describing the simulation scheme.

The approach which was adopted to solve the equations is given below.

1. Specify the geometrical, thermal, and physical parameters as well as the input microwave power, the frequency, and the voltage of the excitation signal.
2. Give an arbitrary temperature.
3. Solve Maxwell's equations.
4. Deduce Q_{ext}.
5. Solve the bio-heat equation and deduce a new value of the temperature.
6. Determine the values of $\varepsilon_r(T)$ and $\sigma(T)$.
7. Repeat steps 3–6 until convergence.
8. Deduce the field $T(t, r, z)$ and other useful quantities.

In order to check the accuracy of our model, the simulation results obtained for the bio-heat model proposed in this work were validated with experimental data obtained by Yang et al. [36]. Figure 6 exhibits the validation related to the temperature distribution in the tissue liver at two positions during the MWA process. These positions are defined by a distance of 4.5 mm or 9.5 mm away from the

antenna. In this case, the microwave was operating at 2.45 GHz with 75 W input power and the initial temperature of the liver tissue was assumed to be 8 °C.

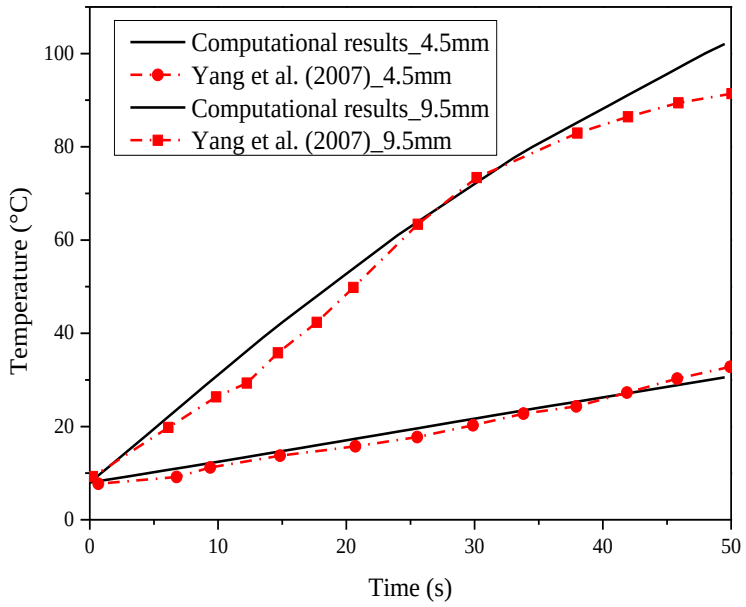

Figure 6. Validation of the temperature distribution in the tissue liver against the experimental data offered by Yang et al. [36].

The results show that the temperature has the same trend as the experimental curve. The difference is very small. This confirms the validation of the present model.

3. Results

As mentioned above, the electromagnetic and bio-heat equations are coupled. The operating frequency of the microwave generated by the antenna was 2.5 GHz. The model is able to be solved using the finite element method. The results mainly concern:

- The microwave power density absorbed by the liver tissue Q_{ext}.
- The specific absorbed rate which is defined as:
- $SAR = \frac{Q_{ext}}{\rho}$, where ρ is the density of the tissue.
- The temperature profile and the maximal values reached.
- The fraction of the tissue necrosis which is related to the tissue damage.

3.1. Absorbed Microwave Power

During thermal ablation of cancer cells, tissue destruction occurs when tissues are heated to sufficient temperatures via a microwave source. The MCA connected to a microwave generator and inserted into the biological tissue is the source of the energy of the microwave. The energy emitted by the antenna propagates into the liver tissue, which allows heat to dissipate in a volume of tissue close to the antenna. This internal heating leads to the killing of cancer cells due to the vibration and rotation of water molecules. It is important to evaluate the microwave power density absorbed by the liver. This quantity is equal to the volumetric source term in the heat equation Q_{ext}.

Figure 7 depicts the microwave power density dissipated in the liver tissue at t = 300 s for three different values of the input microwave power, namely, P_{in} = 10 W, P_{in} = 45 W, and P_{in} = 75 W. For P_{in} = 10 W, the maximal value of the microwave power density is about 34 W/cm^{-3}. However, Q_{ext} carries rapidly through the system. To better observe the spatial variations of Q_{ext}, we limited

the values of this quantity in Figure 7 to the value 1 W/cm^{-3}. In other terms, Figure 7 presents the quantity $\min\left(Q_{ext}, 1\ \mathrm{W/cm^{-3}}\right)$.

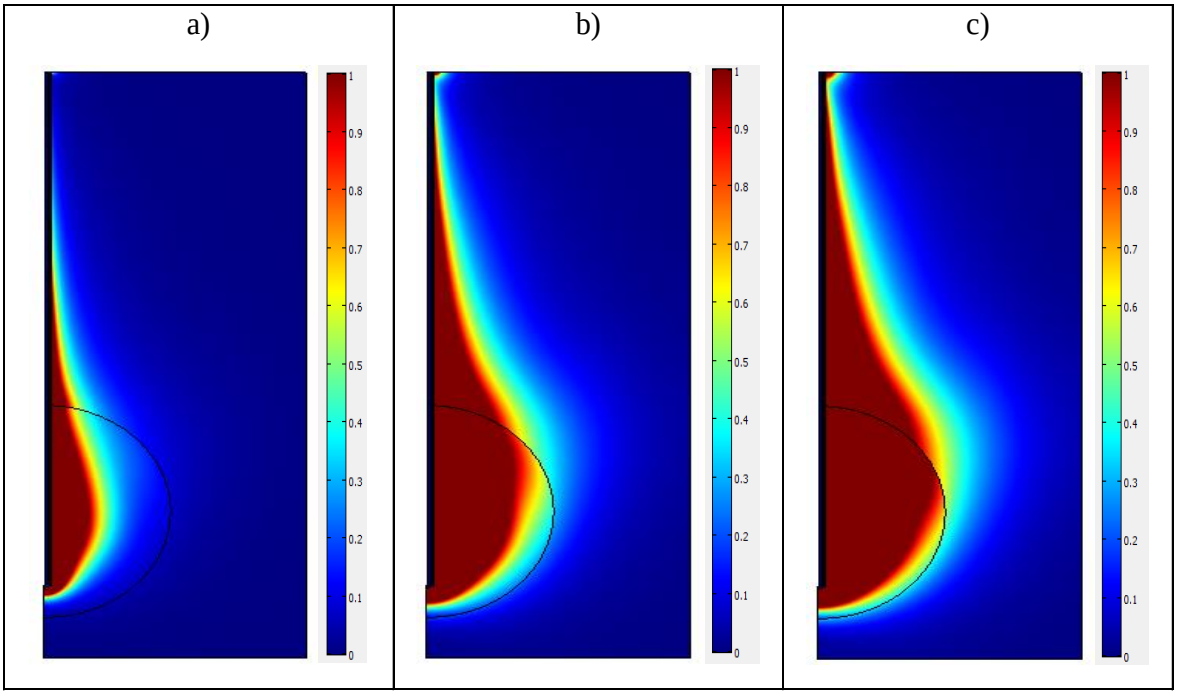

Figure 7. Microwave power density absorbed in liver tissue for various input powers P_{in}: (**a**) $P_{in} = 10$ W, (**b**) $P_{in} = 45$, and (**c**) $P_{in} = 75$ W.

From the above figure it is clear that for the three cases of the power microwave, the microwave power density absorbed is very high near the slot of the antenna and that it decreases with distance. The extension of the heated zone increases with the input power. This extension takes place mainly in the vicinity of the tumor and has an oblong and stretched form.

For $P_{in} = 10$ W, a very small area of the normal tissue is heated, and, at the same time, not all the tumor is heated. When P_{in} increases, all of the tumor is heated, but, unfortunately, a large area of the normal tissue is also heated. A certain compromise should be made to optimize the treatment.

3.2. Specific Absorption Rate Profiles

Through the microwave thermal ablation process the electromagnetic wave propagates into the biological tissue and the energy of this wave is absorbed through the materials. Another interesting parameter is the specific absorption rate, which is defined as the absorbed power density normalized by the tissue density. In order to estimate the ability of heating tissue for different input microwave powers, SAR profiles, at a heating time $t = 300$ s and at a distance of $r = 2.5$ mm from the antenna axis, were generated, and are illustrated in Figure 8.

In this figure, in all cases of microwave power, the SAR profiles show a similar trend with a difference in magnitude. In addition, the SAR increases slowly along the axis parallel to the antenna, reaches a peak around the slot of the antenna, and after this decreases. It is clear that the SAR contour lines have roughly oval and asymmetrical patterns around the slot. The numerical results are in good agreement with those found in [37]. In particular, the SAR distribution for the highest microwave power causes the greatest value of SAR. Moreover, as expected, the maximal SAR value is obtained within the tumor region. The radial profiles at $z = 20$ mm reveal that the SAR increases sharply from the axis. Then, the curves exhibit a hyperbolic decrease. The spatial distribution of SAR can also be presented. The maximal value of SAR for each power is $SAR = 32.7$ kW/kg for $P_{in} = 10$ W, $SAR = 147$ kW/kg for $P_{in} = 45$ W, and $SAR = 245$ kW/kg for $P_{in} = 75$ W.

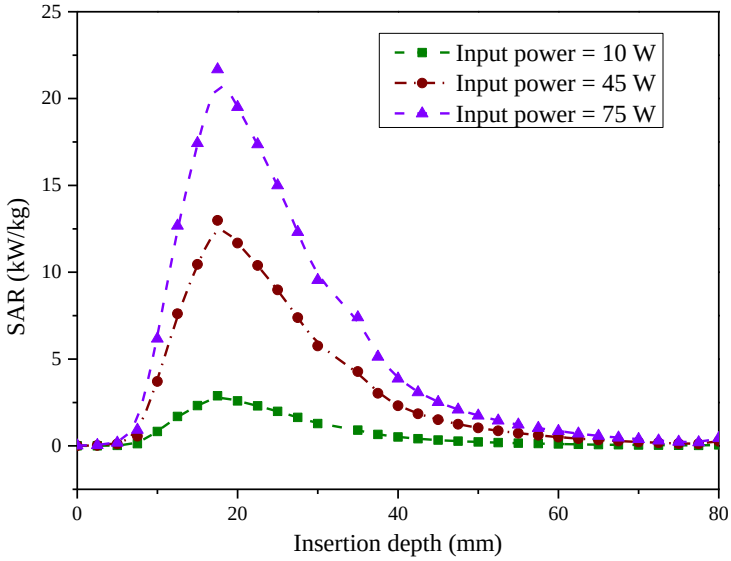

Figure 8. Axial profile of specific absorption rate (SAR) at t = 300 s and r = 2.5 mm for various input powers.

3.3. Temperature and Thermal Gradient Fields

Temperature profile is a major characteristic relating to the effective performance of the MWA. Indeed, microwave ablation should be used as a thermal therapy for cancer tumor treatment without damaging surrounding normal tissue. For this reason, thermal study and temperature control are required.

Figure 9 shows the contours lines of the temperature distribution in the biological tissue at $t = 300$ s for three different values of the input microwave power. It may be noted first that the contour lines of the temperature in the three cases are similar and display an ellipsoidal behavior. The temperature is very high in the vicinity of the antenna slot. Then, it drops noticeably when one moves away from the slot. The maximal temperature value is reached inside the tumor region. The maximum temperature produced by microwave power $P_{in} = 10$ W is estimated to 86 °C, while the maximum value obtained for $P_{in} = 45$ W is 238 °C, and for $P_{in} = 75$ W, the maximum temperature is 353 °C. We note that the temperature increases rapidly when increasing the microwave power. This increase is too high and will destroy healthy cells.

It is also interesting to delimit the region where $\Delta T = T - T_b \geq 15$ °C. For $P_{in} = 10$ W, this region is mainly situated inside the tumor. Hence, there is a very small risk of damaging healthy tissue. The central part of the tumor is killed, however, and the external ring is not completely treated. When P_{in} increases, the area corresponding to $\Delta T \geq 15$ °C becomes larger and more extended than the tumor itself, i.e., it covers the tumor and a part of healthy tissue. Thus, the risk of destroying the tissue surrounding the tumor threatens the process. We may conclude that an input power of about 10 W is sufficient to treat a tumor which has a radius of 15 mm. The results may be extended to deduce the optimal input power required for tumors which have other extensions.

Figure 10 exhibits the temporal evolution of the temperature for different values of the input power and for 4 positions corresponding to $r = 5$ mm, $r = 10$ mm, $r = 15$ mm, and $r = 20$ mm. $z = 20$ mm for all the positions. When the ablation duration is small, the behavior of the curves is mainly governed by the source term. For this reason, a linear increase of the temperature is observed. When the temperature reaches a certain value, the diffusion and the heat conduction due to the blood perfusion become important and lead to a counterbalancing of the source term. Thus, a saturation regime occurs. The maximal values depend on the position and the input power as mentioned above. These curves may help to assess the optimal value of the treatment time.

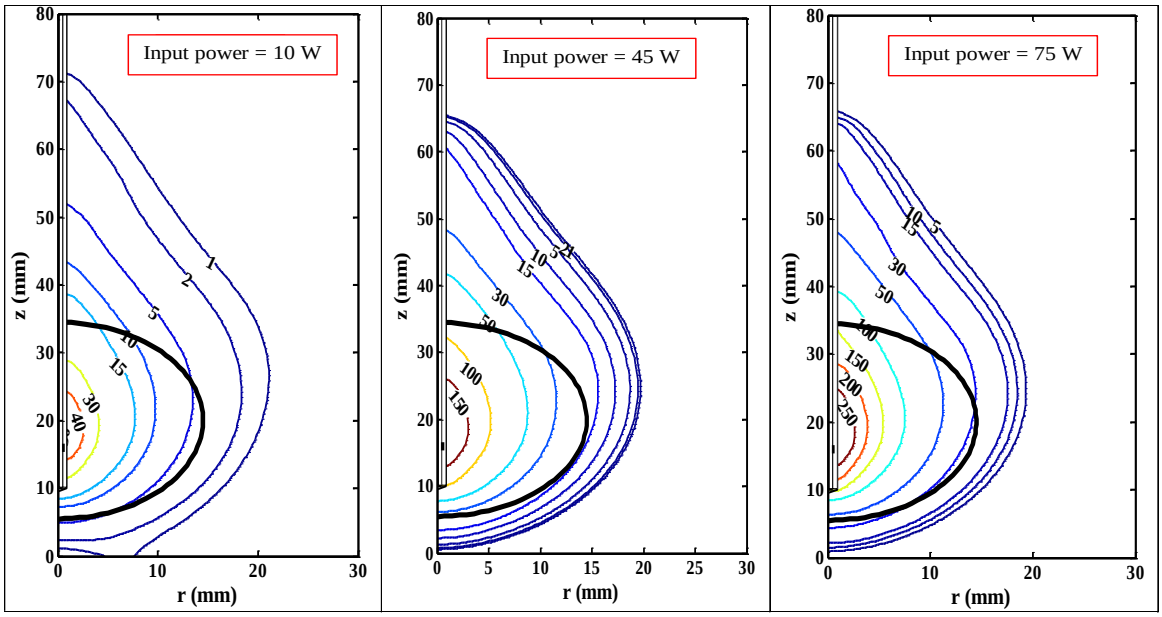

Figure 9. Spatial distribution of ($\Delta T = T - T_{blood}$) for various input powers at t = 300 s.

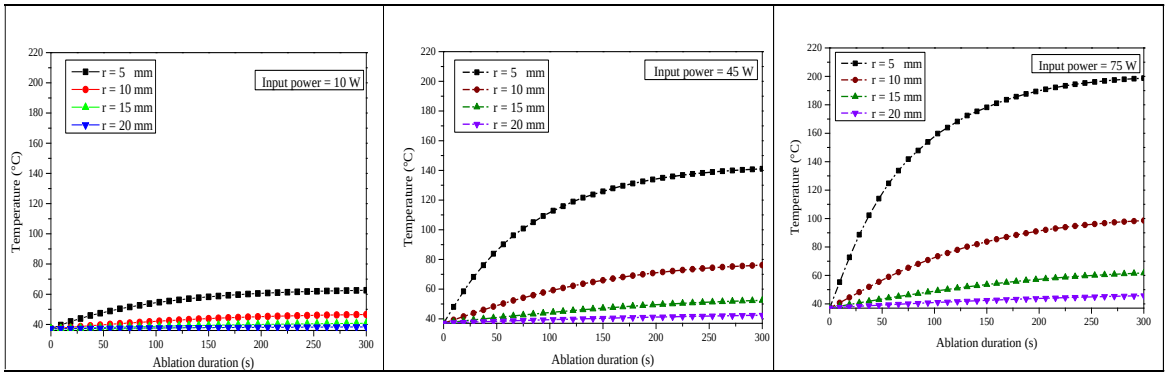

Figure 10. Temporal evolution of the temperature in four positions and for three values of input microwave power.

3.4. The Fraction of Tissue Necrosis

The tissue damage is calculated by an integral using the Arrhenius equation which is written as [38]

$$\alpha = \int_0^t A e^{\frac{-E_a}{RT}}\, dt \tag{15}$$

where α denotes the degree of tissue damage, A is the frequency factor (1/s), and E_a represents the activation energy (J/mol). These two parameters are dependent on the type of the tissue. R is the gas constant and T is the absolute temperature. This integral evaluates the energy accumulated in the tissue over time. In this study, the values $A = 7.39 \times 10^{39}$ (1/s) and $E_a = 2.577 \times 10^5$ (J/mol) were used.

Generally, parameter α is presented through the fraction of tissue necrosis, θ_d, which is expressed as [39]

$$\theta_d = 1 - e^{-\alpha} \tag{16}$$

Figure 11 illustrates the variation in tumor damage during the ablation time for different positions within the liver tissue and for the three input microwave powers. It appears from this figure that the variation in tumor damage varies in the following way: it gradually increases and then reaches a saturation region which presents the completion time of tumor necrosis. It can be clearly seen that

complete tumor necrosis was reached in the three cases for the position r = 0.005 mm away from the antenna after 300 s. From the numerical results, the time required for complete necrosis was found to be 160 s, 60 s, and 40 s for 10 W, 45 W, and 75 W, respectively. Hence, when the microwave power is very high, the time required for complete ablation of the tumor is small. Nevertheless, the probability of damaging normal cells could be high if some care is not taken. The ablation of tumor cells can be achieved over a long period of time without damaging healthy cells when a small input power is used.

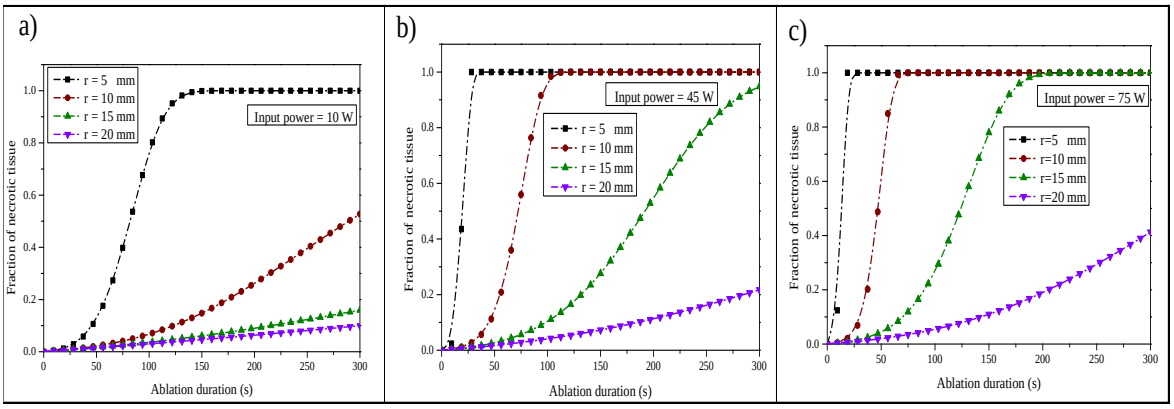

Figure 11. Comparison of the four position fraction of necrotic tissue during the ablation thermal for three values of input microwave power, (**a**) 10 W, (**b**) 45 W and (**c**) 75 W.

4. Conclusions

This paper has dealt with the numerical investigation of conductive and convective heat transfer associated with the propagation of electromagnetic waves in liver tissue during a microwave ablation process for different input microwave powers. The volumetric source term arose from the heat generated by the electromagnetic field since the liver is an electrically conductive material. A numerical simulation was performed using the finite element method to study the absorbed microwave power density, the temperature distribution profile and temporal evolution, the specific absorption rate, and the fraction of necrotic tissue within cancer cells. The results showed that SAR and temperature distribution are strongly affected by input microwave values. In other words, a higher microwave power induces higher SAR values and can increase the temperature to well above 50 °C, which will destroy healthy cells. The SAR pattern and the temperature profile exhibited elongated and asymmetric contour lines centered on the slot. The SAR and the temperature appeared very high near the antenna slot and then decreased by moving away from the antenna axis. The maximum of the SAR and temperature were reached inside the tumor region. The time required for complete necrosis was found to be 160 s, 60 s, and 40 s for 10 W, 45 W, and 75 W, respectively.

In our work, the maximum temperature produced by microwave power $P_{in} = 10$ W was estimated to 86 °C, i.e., the rise temperature $\Delta T = T - T_b = 49$ °C. Furthermore, based on Figure 11, it was found that complete tumor necrosis had been reached only in the case of the position r = 0.005 mm away from the antenna, and the time required for complete necrosis was found to be 160 s for $P_{in} = 10$ W. This power is suitable for a small tumor size. The analysis of this study serves as an essential base for the microwave ablation process and can be used as a guideline for practical treatment. Nevertheless, more care must be taken and a certain compromise should be achieved to kill a maximal part of the tumor while conserving the healthy cells.

Future work will be performed taking into account the size of the tumor with applied input microwave power using a programmable temperature-controlled system by incorporating a proportional-integral-derivative (PID) to better control the temperature distribution.

Author Contributions: M.S. proposed the idea, contributed to data acquisition, and performed the simulation. H.B. performed the algorithm construction. A.A.B.D. contributed to data analysis and the results discussion. All authors have read and agreed to the published version of the manuscript.

Funding: This research received no external funding.

Acknowledgments: The authors would like to thank the Deanship of Scientific Research at Majmaah University for supporting this work under project number No. 38/138.

Conflicts of Interest: The authors declare no competing financial interests.

References

1. Boyle, P.; Levin, B. *World Cancer Report 2008*; WHO: Lyon, France, 2008.
2. Arbyn, M.; Castellsagué, X.; de Sanjosé, S.; Bruni, L.; Saraiya, M.; Bray, F.; Ferlay, J. Worldwide burden of cervical cancer in 2008. *Ann. Oncol.* **2011**, *22*, 2675–2686. [CrossRef] [PubMed]
3. Keangin, P.; Rattanadecho, P.; Wessapan, T. An analysis of heat transfer in liver tissue during microwave ablation using single and double slot antenna. *Int. Commun. Heat Mass Transf.* **2011**, *38*, 757–766. [CrossRef]
4. Al-Dawsari, N.A.; Amra, N. Pattern of skin cancer among Saudi patients attending a tertiary care center in Dhahran, Eastern Province of Saudi Arabia. A 20-year retrospective study. *Int. J. Dermatol.* **2016**, *55*, 1396–1401. [CrossRef] [PubMed]
5. Habash, R.W.; Bansal, R.; Krewski, D.; Alhafid, H.T. Thermal therapy, part 2: Hyperthermia techniques. *Crit. Rev. Biomed. Eng.* **2006**, *34*, 491–542. [CrossRef] [PubMed]
6. Lin, J.C.; Hirai, S.; Chiang, C.L.; Hsu, W.L.; Su, J.L.; Wang, Y.J. Computer simulation and experimental studies of SAR distributions of interstitial arrays of sleeved-slot microwave antennas for hyperthermia treatment of brain tumors. *IEEE Trans. Microw. Theory Tech.* **2000**, *48*, 2191–2198.
7. Rattanadecho, P.; Keangin, P. Numerical study of heat transfer and blood flow in two-layered porous liver tissue during microwave ablation process using single and double slot antenna. *Int. J. Heat Mass Transf.* **2013**, *58*, 457–470. [CrossRef]
8. Kuang, M.; Lu, M.D.; Xie, X.Y.; Xu, H.X.; Mo, L.Q.; Liu, G.J.; Xu, Z.F.; Zheng, Y.L.; Liang, J.Y. Liver cancer: Increased microwave delivery to ablation zone with cooled-shaft antenna—Experimental and clinical studies. *Radiology* **2007**, *242*, 914–924. [CrossRef]
9. Prakash, P.; Salgaonkar, V.A.; Clif Burdette, E.; Diederich, C.J. Multiple applicator hepatic ablation with interstitial ultrasound devices: Theoretical and experimental investigation. *Med. Phys.* **2012**, *39*, 7338–7349. [CrossRef]
10. Haemmerich, D.; Lee, F.T., Jr. Multiple applicator approaches for radiofrequency and microwave ablation. *Int. J. Hyperth.* **2005**, *21*, 93–106. [CrossRef]
11. Liu, Y.J.; Qiao, A.K.; Nan, Q.; Yang, X.Y. Thermal characteristics of microwave ablation in the vicinity of an arterial bifurcation. *Int. J. Hyperth.* **2006**, *22*, 491–506. [CrossRef]
12. Kundu, B. Exact analysis for propagation of heat in a biological tissue subject to different surface conditions for therapeutic applications. *Appl. Math. Comput.* **2016**, *285*, 204–216. [CrossRef]
13. Talaee, M.R.; Kabiri, A.L.I. Analytical solution of hyperbolic bioheat equation in spherical coordinates applied in radiofrequency heating. *J. Mech. Med. Biol.* **2017**, *17*, 1750072. [CrossRef]
14. Deshazer, G.; Prakash, P.; Merck, D.; Haemmerich, D. Experimental measurement of microwave ablation heating pattern and comparison to computer simulations. *Int. J. Hyperth.* **2017**, *33*, 74–82. [CrossRef] [PubMed]
15. Lin, S.-M.; Li, C.-Y. Semi-analytical solution of bio-heat conduction for multi-layers skin subjected to laser heating and fluid cooling. *J. Mech. Med. Biol.* **2017**, *17*, 1750029. [CrossRef]
16. Ierardi, A.M.; Floridi, C.; Fontana, F.; Chini, C.; Giorlando, F.; Piacentino, F.; Brunese, L.; Pinotti, G.; Bacuzzi, A.; Carrafiello, G. Microwave ablation of liver metastases to overcome the limitations of radiofrequency ablation. *Radiol. Med.* **2013**, *118*, 949–961. [CrossRef]
17. Wang, K.; Tavakkoli, F.; Wang, S.; Vafai, K. Analysis and analytical characterization of bioheat transfer during radiofrequency ablation. *J. Biomech.* **2015**, *48*, 930–940. [CrossRef]
18. Ge, M.; Jiang, H.; Huang, X.; Zhou, Y.; Zhi, D.; Zhao, G.; Chen, Y.; Wang, L.; Qiu, B. A multi-slot coaxial microwave antenna for liver tumor ablation. *Phys. Med. Biol.* **2018**, *63*, 175011. [CrossRef]
19. Kabiri, A.; Talaee, M.R. Theoretical investigation of thermal wave model of microwave ablation applied in prostate Cancer therapy. *Heat Mass Transf.* **2019**, *55*, 2199–2208. [CrossRef]

20. Cavagnaro, M.; Amabile, C.; Bernardi, P.; Pisa, S.; Tosoratti, N. A minimally invasive antenna for microwave ablation therapies: Design, performances, and experimental assessment. *IEEE Trans. Biomed. Eng.* **2010**, *58*, 949–959. [CrossRef]
21. Curto, S.; Taj-Eldin, M.; Fairchild, D.; Prakash, P. Microwave ablation at 915 MHz vs 2.45 GHz: A theoretical and experimental investigation. *Med. Phys.* **2015**, *42*, 6152–6161. [CrossRef]
22. Jiang, Y.; Zhao, J.; Li, W.; Yang, Y.; Liu, J.; Qian, Z. A coaxial slot antenna with frequency of 433 MHz for microwave ablation therapies: Design, simulation, and experimental research. *Med. Boil. Eng. Comput.* **2017**, *55*, 2027–2036. [CrossRef] [PubMed]
23. Biffi Gentili, G.; Ignesti, C.; Tesi, V. Development of a novel switched-mode 2.45 GHz microwave multiapplicator ablation system. *Int. J. Microw. Sci. Technol.* **2014**, *2014*, 973736. [CrossRef]
24. Sebek, J.; Albin, N.; Bortel, R.; Natarajan, B.; Prakash, P. Sensitivity of microwave ablation models to tissue biophysical properties: A first step toward probabilistic modeling and treatment planning. *Med. Phys.* **2016**, *43*, 2649–2661. [CrossRef] [PubMed]
25. Wang, T.; Zhao, G.; Qiu, B. Theoretical evaluation of the treatment effectiveness of a novel coaxial multi-slot antenna for conformal microwave ablation of tumors. *Int. J. Heat Mass Transf.* **2015**, *90*, 81–91. [CrossRef]
26. Rubio, M.F.; López, G.D.; Perezgasga, F.V.; García, F.F.; Hernández, A.V.; Salas, L.L. Computer Modeling for Microwave Ablation in Breast Cancer Using a Coaxial Slot Antenna. *Int. J. Thermophys.* **2015**, *36*, 2687–2704. [CrossRef]
27. Karampatzakis, A.; Kühn, S.; Tsanidis, G.; Neufeld, E.; Samaras, T.; Kuster, N. Heating characteristics of antenna arrays used in microwave ablation: A theoretical parametric study. *Comput. Boil. Med.* **2013**, *43*, 1321–1327. [CrossRef]
28. Pennes, H.H. Analysis of tissue and arterial blood temperatures in the resting human forearm. *J. Appl. Physiol.* **1998**, *85*, 5–34. [CrossRef]
29. Sturesson, C.; Andersson-Engels, S. A mathematical model for predicting the temperature distribution in laser-induced hyperthermia. Experimental evaluation and applications. *Phys. Med. Biol.* **1995**, *40*, 2037–2052. [CrossRef]
30. Yang, D.; Converse, M.C.; Mahvi, D.M.; Webster, J.G. Measurement and analysis of tissue temperature during microwave liver ablation. *IEEE Trans. Biomed. Eng.* **2006**, *54*, 150–155. [CrossRef]
31. Shi, J.; Chen, Z.; Shi, M. Simulation of heat transfer of biological tissue during cryosurgery based on vascular trees. *Appl. Therm. Eng.* **2009**, *29*, 1792–1798. [CrossRef]
32. Brace, C.L. Temperature-dependent dielectric properties of liver tissue measured during thermal ablation: Toward an improved numerical model. In Proceedings of the 2008 30th Annual International Conference of the IEEE Engineering in Medicine and Biology Society, Vancouver, BC, Canada, 20–25 August 2008.
33. Wessapan, T.; Srisawatdhisukul, S.; Rattanadecho, P. Specific absorption rate and temperature distributions in human head subjected to mobile phone radiation at different frequencies. *Int. J. Heat Mass Transf.* **2012**, *55*, 347–359. [CrossRef]
34. Hadizafar, L.; Azarmanesh, M.N.; Ojaroudi, M. Enhanced bandwidth double-fed microstrip slot antenna with a pair of l-shaped slots. *Prog. Electromagn. Res.* **2011**, *18*, 47–57. [CrossRef]
35. Chen, Z. *Finite Element Methods and Their Applications*; Scientific Computation; Springer: Berlin, Germany, 2005.
36. Yang, D.; Converse, M.C.; Mahvi, D.M.; Webster, J.G. Expanding the bioheat equation to include tissue internal water evaporation during heating. *IEEE Trans. Biomed. Eng.* **2007**, *54*, 1382–1388. [CrossRef] [PubMed]
37. Saito, K.; Taniguchi, T.; Yoshimura, H.; Ito, K. Estimation of SAR distribution of a tip-split array applicator for microwave coagulation therapy using the finite element method. *IEICE Trans. Electron.* **2001**, *84*, 948–954.
38. Singh, S.; Repaka, R. Effect of different breast density compositions on thermal damage of breast tumor during radiofrequency ablation. *Appl. Therm. Eng.* **2017**, *125*, 443–451. [CrossRef]
39. Jasinski, M. Investigation of tissue thermal damage process with application of direct sensitivity method. *Mol. Cell. Biomech.* **2013**, *10*, 183–199. [PubMed]